Motor properties from persistence: a linear molecular walker lacking spatial and temporal asymmetry

2015 New J. Phys. 17 055017

(http://iopscience.iop.org/1367-2630/17/5/055017)

New Journal of Physics
The open access journal at the forefront of physics

Deutsche Physikalische Gesellschaft DPG
IOP Institute of Physics

Published in partnership with: Deutsche Physikalische Gesellschaft and the Institute of Physics

OPEN ACCESS

RECEIVED
25 February 2015

REVISED
25 March 2015

ACCEPTED FOR PUBLICATION
13 April 2015

PUBLISHED
15 May 2015

PAPER

Motor properties from persistence: a linear molecular walker lacking spatial and temporal asymmetry

Martin J Zuckermann[1], Christopher N Angstmann[2], Regina Schmitt[3], Gerhard A Blab[4], Elizabeth HC Bromley[5], Nancy R Forde[1], Heiner Linke[3] and Paul MG Curmi[6]

[1] Department of Physics, Simon Fraser University, 8888 University Drive, Burnaby, BC, V5A 1S6, Canada
[2] School of Mathematics and Statistics, University of New South Wales, Sydney NSW 2052, Australia
[3] Solid State Physics and Nanometer Structure Consortium (nmC@LU), Lund University, PO Box 118, SE 221 00 Lund, Sweden
[4] Molecular Biophysics, Universiteit Utrecht, Utrecht, The Netherlands
[5] Department of Physics, University of Durham, Durham, UK
[6] School of Physics, University of New South Wales, Sydney NSW 2052, Australia

E-mail: nforde@sfu.ca **and** p.curmi@unsw.edu.au

Keywords: molecular motor, Brownian ratchet, kinesin, Langevin dynamics, artificial protein motor, feedback control

Supplementary material for this article is available online

Abstract

The stepping direction of linear molecular motors is usually defined by a spatial asymmetry of the motor, its track, or both. Here we present a model for a molecular walker that undergoes biased directional motion along a symmetric track in the presence of a temporally symmetric chemical cycle. Instead of using asymmetry, directionality is achieved by persistence. At small load force the walker can take on average thousands of steps in a given direction until it stochastically reverses direction. We discuss a specific experimental implementation of a synthetic motor based on this design and find, using Langevin and Monte Carlo simulations, that a realistic walker can work against load forces on the order of picoNewtons with an efficiency of ~18%, comparable to that of kinesin. In principle, the walker can be turned into a permanent motor by externally monitoring the walker's momentary direction of motion, and using feedback to adjust the direction of a load force. We calculate the thermodynamic cost of using feedback to enhance motor performance in terms of the Shannon entropy, and find that it reduces the efficiency of a realistic motor only marginally. We discuss the implications for natural protein motor performance in the context of the strong performance of this design based only on a thermal ratchet.

1. Introduction

Motion is an essential feature of all living systems. Both macroscopic and molecular scale biological motion is effected by protein complexes. These motor proteins transduce chemical energy, often in the form of ATP hydrolysis, into mechanical work [1]. There is a vast array of motor proteins that cover a wide gamut of performance characteristics from rapid motion to high output work [2–7]. A full physical understanding of how these motor proteins transduce energy is still under development.

Several physical characteristics are common to biological motors. The tracks along which linear motors move tend to be asymmetric or directional. The motors work under non-equilibrium conditions so that the energizing chemical reactions are essentially irreversible, and they rectify thermal fluctuations to achieve stepping [8–14]. Some biological motors appear to operate as Brownian ratchets [15–17], while others, such as conventional linear motors, may implement a 'power stroke' [18, 19] to induce long-range steps [20].

While the majority of work on molecular motors consists of studying natural motors and their variants, a synthetic biology approach espouses the design and construction of artificial motors [21–26]. Using this approach in combination with modeling, it is possible to focus on one principle at a time and address possible physical mechanisms.

In essentially all known biological motors, directionality is established by a combination of track asymmetry (actin filaments, microtubules, single DNA strands) and structural changes in the motor protein (myosin, kinesin, helicases). Similarly, molecular motors in the nascent synthetic field generally have directionality imposed through asymmetric track design [21, 22, 24, 25, 27]. Alternatively, symmetric tracks and motors have been demonstrated to give rise to persistent directed motion following an initially random choice of translocation direction; these motors modify their tracks to establish and maintain local asymmetry as part of the motility mechanism [28–31]. Experimental realizations of such symmetric motors have not yet succeeded in implementing a refreshable track, meaning that these motors can follow the path once only.

Here we introduce the concept of a molecular walker that can move persistently over substantial distances *in the absence of spatial or temporal asymmetry*. The walker is bi-directional, but once a starting configuration is established, it maintains its direction of motion over many steps. Furthermore, it does not alter its track, meaning that the track can be reused for further trajectories. We call this walker synthetic kinesin-inspired protein (SKIP) because it is inspired by kinesin's use of restricted diffusional search for forward binding to its microtubule track [1–7], using the binding orientation of one 'foot' to spatially constrain the diffusional search of the second foot to the forward-binding site. In this manner, it bears similarity to an earlier proposed bipedal design [26], but by contrast SKIP walks on a symmetric rather than polar track. Powered by changes in chemical potential, SKIP has no power stroke, and utilizes only diffusive motion to achieve motility, thus permitting a test of the efficiency with which a thermal ratchet can execute useful work. Through the use of Langevin and Monte Carlo simulations, we explore the mechanism of this walker, and determine its performance as a molecular motor.

Our simulations show that for well chosen parameters, SKIP can persistently move unidirectionally for hundreds of steps before stochastically reversing its direction against load forces comparable to several $kT/2d$, where kT represents the thermal energy of the system and $2d$ is SKIP's step size (figure 1). By suitable track design, the walker can be made to reverse direction automatically at the end of the track, thereby turning the walker into a shuttle.

From a physics point of view, it is interesting to note that SKIP is fundamentally a feedback motor: to apply a load force, and thus to turn the walker into a motor, the walker's initial direction of motion must be known. While this could be established initially by track engineering at one end, because SKIP can spontaneously reverse its direction of motion, it is useful to adjust the direction of load force in real time, similar to a Maxwell demon. In this way, SKIP's ability to do accumulated work can be made arbitrarily large up to a maximal load force where it stalls. We explore the energetics of this system and find that the thermodynamic cost of feedback only marginally reduces the efficiency of a realistic implementation of SKIP because it is small compared to the free energy required to power the motor.

Using parameters for a specific and feasible experimental implementation of the SKIP motor (based on ligand-gated DNA-binding proteins and a DNA track), we are able to compare its performance to that of kinesin, the prototypical linear molecular motor protein. Impressively, we find that SKIP's run length under a load force of 1 pN and its efficiency are comparable to that of kinesin. SKIP thus presents not only a new class of motor (a symmetric motor that maintains directionality exclusively by persistence), but also demonstrates that a fully diffusive motor with an experimentally achievable design can perform approximately as well as biological motors.

2. Model concept and design

2.1. Detailed description of the SKIP walker concept

As conceived, SKIP comprises a linear arrangement of four gated track-binding modules (A and B in figure 1(a)) where A (B) modules only bind a (b) sites on a linear track in the presence of the activating ligand, l_a (l_b). This dependence of track-binding on ligand occupancy of each foot module can be thought of akin to ATP-powered motors, whose track binding is modulated by occupancy of the ATP site [1, 2]. The separation between identical track-binding modules, d, is equal to the site separation on the track, while the separation between the central protein modules A_2 and B_2 is chosen to be shorter ($e < d$). This shorter central link is critical in achieving directional persistence [26]. The track consists of a periodic linear arrangement of binding motifs a_1–a_2–b_1–b_2 where the two a (b) motifs are identical (figure 1(a)).

While the following model is quite general, it is helpful to have a specific experimental implementation of the SKIP walker in mind. For example, modules A and B can be thought of as two different, ligand-gated DNA-binding repressor proteins. The physical properties of such repressor proteins that are relevant to their use as artificial motor modules have been described in detail for our previous design, the tumbleweed [24]. The linear track may then be implemented as a synthetic DNA molecule with specific binding sites a and b [24, 32]. The spacing between adjacent sites on the track, d, is set at 10 nm (table 1) to accommodate repressor binding [24].

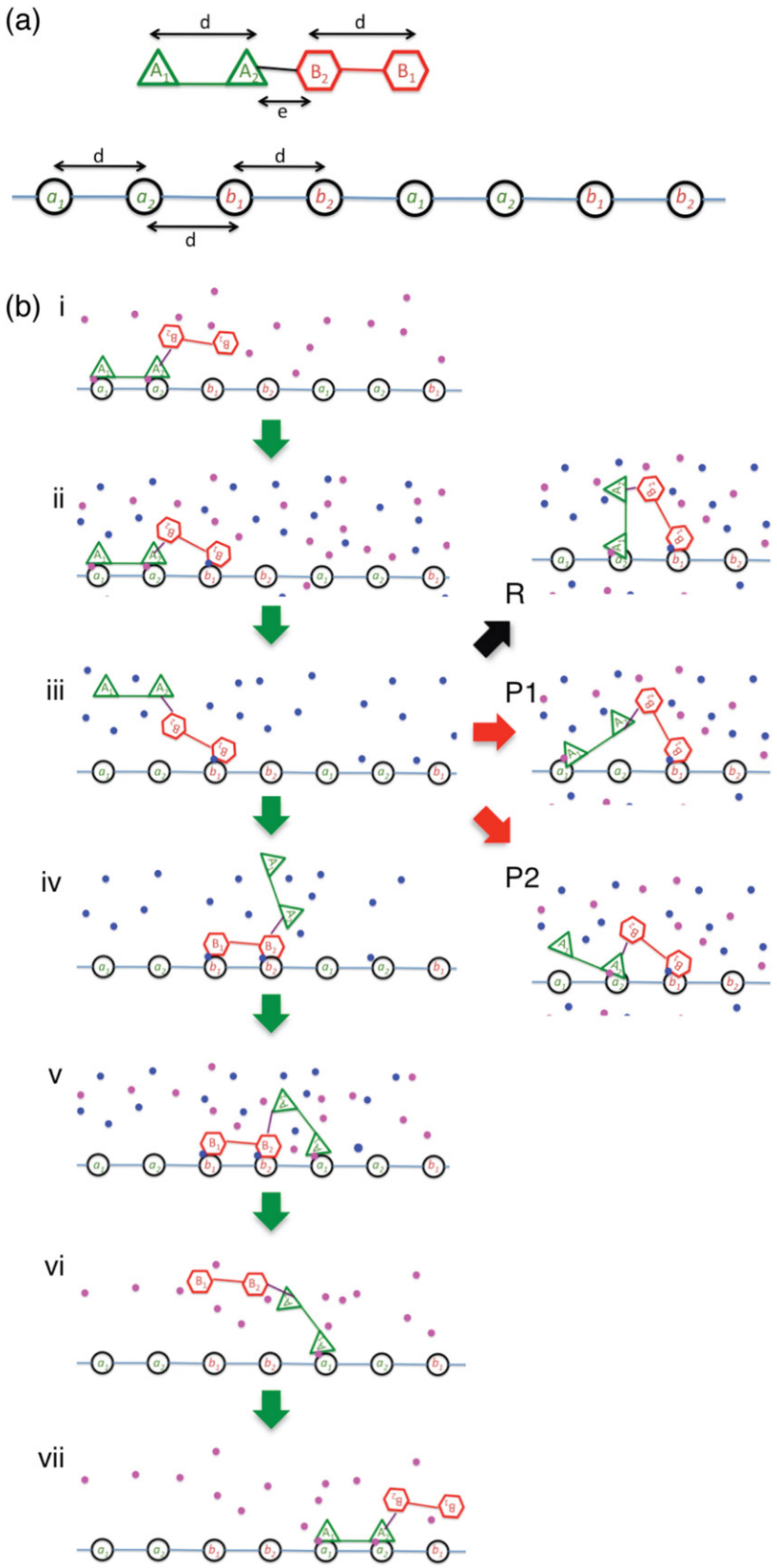

Figure 1. *Design of SKIP.* (a) Model of SKIP (top) and its track (bottom). (b) Configurations during one full cycle (four ligand pulses) for ideal directional and processive forward motion of the motor (i)–(vii). The steps between states (i)–(iv) represent one half-cycle starting with the *A* modules bound and ending with *B* modules bound, during which SKIP translocates forward a distance of 2*d*. The steps between states (iv)–(vii) are the second half-cycle starting with *B* bound and ending with *A* bound. Adjacent to the vulnerable state with only a single module *B* bound (state (iii)) are shown transitions in the subsequent ligand pulse leading to unsuccessful forward motion (right column, R, P1, P2). An equivalent set of non-productive states could occur from the second vulnerable state with only a single module *A* bound (state (vi)), however, these are not shown. The track-binding modules are labeled by capital letters, the binding sites on the track are labeled by small letters, the l_a ligands for the *A* track-binding modules are shown as magenta dots and the l_b ligands for the *B* track-binding modules are shown as blue dots.

Table 1. Model parameters.

Parameter	Symbol	Value
Long bond in motor	d	10 nm
Short bond in motor	e	5 nm
Thermal energy	kT	4.1 pN nm
Drag coefficient of each track-binding module sphere	γ	2.6×10^{-11} kg s^{-1}
Track-binding module 'sphere' radius	r	1.25 nm
Effective range of specific binding	d_b	1.5 nm
Interaction strength of specific binding potential	V_S	4.1×10^3 pN nm
Interaction strength of harmonic potential	V_H	1.31×10^3 pN nm^{-1}
Interaction strength of Lennard–Jones potential	V_{LJ}	98.4 pN nm
Lennard–Jones distance parameter	σ	2.5 nm
Langevin time step	Δt	7.2 ps

The binding sites for repressors on DNA have palindromic sequences, hence the DNA track will be symmetric. Using a microfluidic device to temporally change the concentration of ligands [33], the binding and unbinding of modules A and B to the track can be orchestrated in arbitrary temporal order.

SKIP motility is then driven by changing the concentration of the ligand(s) bathing the track (figure 1(b)). Hence SKIP is essentially a clocked walker where each ligand condition is maintained for a period known as the ligand pulse time (τ_{LP}) and set by the repetitive sequence: (l_a, 0)-(l_a, l_b)-(0, l_b)-(l_a, l_b). This series of four ligand pulses is sufficient to power one complete forward cycle of SKIP, as illustrated in figure 1(b).

Consider the specific starting condition where initially the two A modules are bound to the track in the presence of ligand l_a only (figure 1(b), state (i)). When ligand l_b is added, only protein module B_1 is able to bind to the track, and only at the b_1 site nearest the bound A modules, due to the geometrical constraint that $e < d$ (see figure 1(b), state (ii)). This geometrical constraint is one key aspect of SKIP's persistence mechanism, and was inspired by the restricted diffusional search of kinesin's forward head (which, in kinesin's case, follows a power stroke). On removing ligand l_a, SKIP remains attached to the track by a single module B_1 (figure 1(b), state (iii)).

We call state (iii) in figure 1(b) the vulnerable state, and the future behavior of the walker is dependent on what happens at this stage: it may step forward, pause or reverse. If module B_2 binds to the track at the adjacent b_2 site, then SKIP has taken a half step forwards, moving a distance of $2d$ along the track in the time of $2\tau_{LP}$ (figure 1(b), state (iv)). Here, the binding of B_2 occurs through diffusion, while in kinesin, the 'throw-forward' motion that positions the head for forward binding is driven by the allosteric power stroke [2].

If no track binding has occurred by the time ligand l_a is reintroduced, SKIP may yet succeed in forward-binding (figure 1(b), state (iv)) or take one of three additional actions. The first is that the motor may pause by returning to the initial state (figure 1(b), state (ii)) if either A module binds to its previous track site (figure 1(b), P1 and P2). If this happens, SKIP is out of sync with the ligand pulses and only after an additional $2\tau_{LP}$ can it resume forward motion. Alternatively, the motor may reverse its direction of travel, which happens if motor module A_1 binds to the track at the a_2 site nearest the bound B_1 motor module (figure 1(b) R). We observe this initial binding always to be followed by binding of A_2 at the a_1 site in the following (l_a, 0) ligand pulse when load is present, thus leading to reversal and a mirror image of state (i).

It is important to note that the SKIP cycle, the track and the ligand-pulse sequence (l_a, 0)-(l_a, l_b)-(0, l_b)-(l_a, l_b) are all symmetric, and the track is not modified by SKIP stepping. A direction of motion is defined only by the initial binding configuration of SKIP. As we will show below, a SKIP in forward (reverse) facing configuration has a large likelihood of continuing to move in the same direction for many steps in sequence. It is also important to note that stepping is entirely diffusive as no power stroke is present in the model. The motor is powered by changes in the chemical potential of the ligand bath, the corresponding energy input of which is quantified below.

2.2. Langevin simulations

To investigate the behavior of SKIP, we simulated its motion using three-dimensional coarse-grained Langevin dynamics [24, 34]. SKIP is represented by a freely jointed linear tetramer composed of three stiff bonds connecting four spheres, each representing a track-binding module. We use the indices $j = 1 \ldots 4$ to designate the four SKIP repressors: $1 \equiv A_1$, $2 \equiv A_2$, $3 \equiv B_1$ and $4 \equiv B_2$ (figure 1(a)). Let $\Delta x_i^{(j)}$ be the change in the value of the ith coordinate ($i = 1, 2, 3$) of the jth track-binding module over an incremental time, Δt, at time t. The overdamped Langevin equation can then be written as follows:

$$\Delta x_i^{(j)} = F_i^{(j)} \Delta t/\gamma + (2kT\Delta t/\gamma)^{1/2} \zeta_i^{(j)}(t), \quad (1)$$

where $F_i^{(j)}$ is the ith component of the sum of an internal conservative force, $F_{Ci}^{(j)}$, and an external force, $F_{Ei}^{(j)}$, on the jth track-binding module at time t. γ is the drag coefficient for each monomer and is given by the Stokes–Einstein equation in terms of the radius, r, of the monomeric sphere and the viscosity, η, of the buffer: $\gamma = 6\pi\eta r$. The last term in equation (1) models thermal noise. $\zeta_i^{(j)}(t)$ is a random number taken from a Gaussian distribution with zero mean where

$$\left\langle \zeta_i^{(j)}(t) \cdot \zeta_{i'}^{(j')}(t') \right\rangle = \delta_{ii'}\delta_{jj'}\delta(t-t') \tag{2}$$

$F_{Ci}^{(j)}$ acts on each monomer and is the negative gradient of a potential given by $W_H + W_{SB} + W_{LJ}$. Here W_H is a harmonic potential which defines the lengths d and e of the three bonds between the track-binding modules of SKIP. W_{SB} is the specific binding potential present at all binding sites on the track. The track is taken to lie along the x_1-axis and the specific binding potential for a track-binding module of type j to its specific recognition sequences is given by $W_{SB}(r_j) = -V_{SB}\exp\left(-r_j^2/d_b^2\right)$ for $r_j < d_b$. Here V_{SB} is the strength of the specific binding interaction, d_b is its effective range and r_j is the distance between track-binding module j and the nearest corresponding recognition sequence on the track. To model the case where a ligand is absent from solution, this specific binding potential is turned off by making $W_{SB}(r_j) = 0$. W_{LJ} is the excluded volume between two track-binding modules and is simulated by a repulsive Lennard–Jones interaction in terms of the minimum distance, σ, between the centers of two spherical monomers representing the track-binding modules.

The components of the external force, $F_{Ei}^{(j)}$, which is used to model a load force on SKIP, are taken to be parallel to the track and act only on monomers A_2 and B_2. Unless otherwise stated, the load force is applied in the negative direction (to the left in figure 1(b)), and the total external force, F_{ext} (the sum of the forces on A_2 and B_2) is reported. This load force is taken to represent an external force applied, for example, by optical tweezers or by an imposed fluid flow at constant velocity, and is distinct from a Stokes drag force caused by an actual load tethered to SKIP, which results in qualitatively different and more complex behavior.

The specific numerical parameters used in the simulations are listed in table 1, and are motivated by realistic values for an experimental implementation using repressor proteins and a DNA track (see [24] and above).

The ligand pulse time, τ_{LP}, was varied between 0.03 and 1.152 ms. The lower limit is set by the time SKIP needs to diffuse from the state with two modules bound (states (i) or (iv) in figure 1(b)) to that with three modules bound (states (ii) or (v) in figure 1(b)). When $\tau_{LP} > 0.03$ ms, SKIP is processive under zero load (see below). It was not feasible to model $\tau_{LP} > 1.152$ ms, timescales that would more closely mimic kinesin's step time ($\sim$10 ms at saturating ATP) [35, 36]. The τ_{LP} accessible in experiments can be expected to be $\gg$1 ms.

For all simulations, the motor is started in state (ii) (figure 1(b)). Changes in ligand concentrations are modeled by turning the corresponding binding potentials on or off. Binding of a monomer occurs if it happens to diffuse within a distance d_b of an active binding site. The value of V_{SB} has been chosen large enough to ensure that, once bound, a monomer does not unbind until the corresponding specific binding potential is turned off.

Langevin simulations were also used to model the behavior of SKIP under feedback control, where feedback was used to reverse the direction of the load force following reversal of SKIP on its track. The calculation of the work done by SKIP under feedback control is performed in the following manner in the Langevin simulations. We begin by assuming that SKIP is in the forward-facing configuration (either states (ii) or (v) in figure 1(b)) at ligand pulse n under a total rearward (load) force $F_{ext} < 0$. Then there are three possibilities.

(i) If SKIP advances two lattice spacings to the next forward-facing configuration (equivalent to states (v) or (ii) in figure 1(b)) at ligand pulse $n + 2$, the work done by SKIP against the rearward force is given by $F_{ext}{}^{*}2d$, which is added to the total work performed so far.

(ii) If SKIP reverses its direction via the configuration shown in figure 1(b) R, its configuration after a full ligand cycle (at ligand pulse $n + 4$) becomes reverse facing (i.e., a mirror image of either states (ii) or (v) in figure 1(b)), and the position of SKIP's center of mass is changed, on average, by $1.062d$ in the reverse direction, based on the geometry of the motor. In this case the work done by the rearward force is $1.062d^{*}$ F_{ext}. This is subtracted from the total work performed so far and the external force is reversed at this point in the simulation run, i.e., F_{ext} is replaced by $-F_{ext}$.

(iii) If SKIP's position is unchanged via one of the configurations shown in figure 1(b) P1 and P2 after two τ_{LP} (pausing), no work was done.

If SKIP is in a reverse-facing configuration at ligand pulse n with a forward external force, the same three possibilities exist for work output in the mirrored transitions.

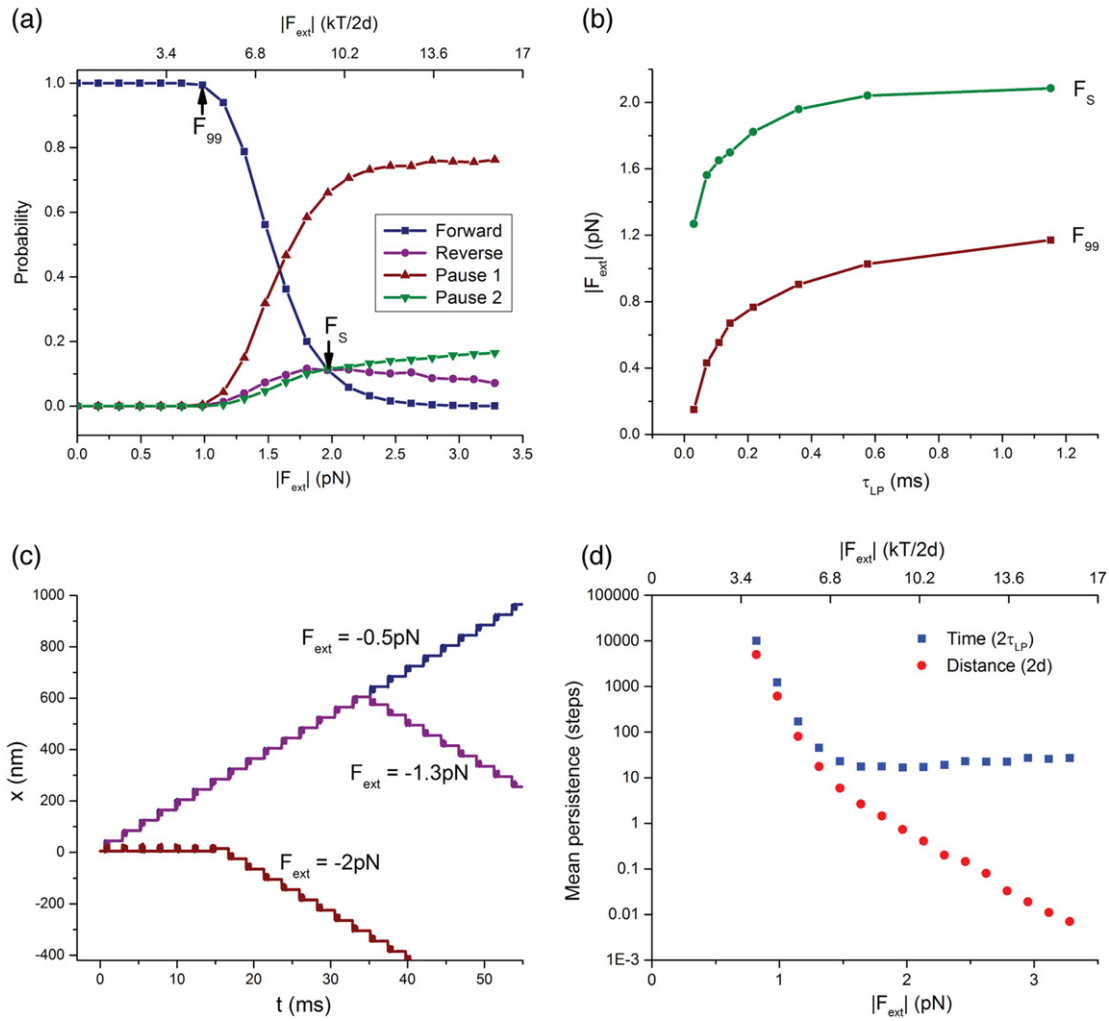

Figure 2. *Force-dependence performance of SKIP.* (a) Probabilities of transitions as a function of rearward force, $F_{ext} < 0$. During the first τ_{LP}, only the forward transition is allowed (blue squares). If this transition does not occur by the end of this pulse cycle (e.g. for $F > F_{99}$), then other processes contribute in the next pulse cycle, leading to motor stall (red and green triangles correspond to pauses P_{P1} and P_{P2}, respectively) or reversal (magenta circles). The units of force are displayed both in units of pN and in non-dimensional units of $kT/2d$. The values of F_{99} and F_S are indicated by black arrows. (b) The maximum force against which translocation occurs increases as a function of τ_{LP}. The upper (green) curve shows F_S, the force at which the probability for the forward transition equals the probability of reversal in a given step, while the lower curve (red) shows F_{99}, the force at which there is a 99% probability that the motor continues to move forwards at each step. (c) Sample motor trajectories, illustrating persistent motion, reversal under force and extended stalling under force with increasing load force. The three trajectories shown are for the following rearward forces: −0.5 pN (2.4 $kT/2d$), −1.3 pN (6.4 $kT/2d$), −2 pN (9.6 $kT/2d$). (d) The mean persistence distance (red circles) and time (blue squares) are plotted as a function of external force. The mean persistence distance is expressed in units of motor steps, $2d$, while the mean persistence time is in units of $2\tau_{LP}$. Persistence values were determined by Monte Carlo simulations, using the probabilities of panel (a). For panels (a), (c) and (d) $\tau_{LP} = 0.576$ ms.

2.3. Monte Carlo simulations

Monte Carlo simulations were undertaken to investigate the role of the vulnerable state on the processivity of SKIP and to characterize the effect of feedback on motor efficiency. The probabilities of the four possible transitions from the vulnerable state (state (iii) in figure 1(b)) were used as input: P_F, P_{P1}, P_{P2} and P_R, for forward (iii)–(iv), pausing and reverse transitions. These probabilities were determined from the Langevin simulations for each force and value of τ_{LP} under investigation (see figure 2(a)). If the forward transition occurred, we assumed that this transition always leads to productive forward motion, so the position of SKIP was changed by $2d$ upon forward translocation, the time was advanced by $2\tau_{LP}$, and the choice among P_F, P_{P1}, P_{P2} and P_R recurred for the next step. In this case, the work performed by SKIP was $F_{ext}{}^{*}2d$, taken to be positive since this motion occurred against the applied force. If a pause transition was selected, the position of SKIP remained unchanged, no work was performed, and the time was updated by $4\tau_{LP}$, as a full cycle was needed before forward motion would become in sync with the externally regulated ligand supply. Finally, if a reverse transition was selected, we assumed this would always lead to a reverse-facing SKIP configuration (mirror image of state (i)), and consequently the walker's position was changed by $-1.062d$. The time was then updated by $4\tau_{LP}$, the time required to achieve this full reorientation of the walker. The work performed by SKIP was $-|F_{ext}|{}^{*}1.062d$, and at

this point, the direction of the external force was reversed, so that it again applied a load to SKIP, whose direction was taken to be the 'new' forward.

3. Motor performance

3.1. Force-dependence of transitions

We investigated the force-dependent probability of different steps in the walker's cycle by Langevin simulations, recording first-passage times (FPT) for transitions from state (ii) (see figure 1(b)) following the removal of ligand l_a, which results in the unbinding of A-type track-binding modules and SKIP entering the vulnerable state (iii). Figure 2(a) shows a representative set of force-dependent probabilities for $\tau_{LP} = 0.576$ ms. At low external force, the diffusive search process is fast enough that the probability of executing the forward step during τ_{LP} remains near unity, even as this rearward force increases. When the force exceeds about $5kT/2d$ for this τ_{LP}, the forward probability decreases rapidly with increasing rearward force as the transition from states (iii) → (iv) is increasingly inhibited within τ_{LP}. This provides access to other processes (pause 1, pause 2 and reversal, labeled P1, P2 and R in figure 1(b)) in the subsequent ligand environment (l_a, l_b).

To characterize the force at which the forward probability starts to decrease we define F_{99} as the force at which the forward transition decreases to a 99% probability. As a proxy for a stall force, we define F_S as the force at which forward and reverse transitions are equally probable (figure 2(a)). The values of F_{99} and F_S depend on τ_{LP}: for longer ligand pulse durations, the motor has more chance to forward-bind, and can execute this transition under increasing load (figure 2(b)). The shapes of the transition probability curves in figure 2(a) only change substantially as τ_{LP} becomes shorter than the FPT: at sufficiently short times, SKIP may not successfully move forward even at zero load ($P_F < 1$), and there is a small but finite probability of detachment (supporting figure 1 available at stacks.iop.org/NJP/17/055017/mmedia).

We note that for very high rearward forces, pausing is predicted from the probabilities (figure 2(a)) to dominate, keeping the walker stationary on the track. This is also visible in the initial part of the trajectory for $F_{ext} = -2$ pN in figure 2(c). It is worth noting that SKIP's force tolerance is remarkably high for a purely diffusive motor. For the value of $\tau_{LP} = 0.576$ ms, we find $F_{99} \cong -1$ pN or $\sim -5\ kT/2d$, where $kT/2d$ is the natural force scale of a diffusive motor with SKIP's step size, $2d$. We discuss a comparison between SKIP and the natural protein motor kinesin at the conclusion of this paper.

3.2. Persistent random walker

As predicted by the force-dependent transition probabilities, SKIP behaves as a persistent walker under low rearward force, stepping processively in the forward direction established by its initial bound configuration on the track (figure 2(c) and supporting movie available at stacks.iop.org/NJP/17/055017/mmedia). It occasionally pauses, however, before resuming forward motion or reversing. The latter is shown in figure 2(c) ($F_{ext} = -6.4\ kT/2d$ or -1.3 pN). As F_{ext} increases in magnitude, SKIP is more likely to undergo pause and reversal, doing so earlier in its run. Finally, under sufficiently large forces (for $\tau_{LP} = 0.576$ ms, $|F_{ext}| > \sim 8\ kT/2d$ or ~ 1.6 pN), pausing dominates as predicted by figure 2(a), leading to long-lived stationary paused states before the walker eventually reverses direction (e.g. $|F_{ext}| = 2$ pN in figure 2(c)). Under any force, once the direction of motion is aligned with the external force, the motor undergoes unidirectional processive motion assisted by this force (figure 2(c)).

The persistent run length of SKIP is remarkably high and depends both on the load force, F_{ext}, and τ_{LP}. Figure 2(d) shows the mean persistence time (number of $2\tau_{LP}$) and distance (number of $2d$ steps) as a function of load force for $\tau_{LP} = 0.576$ ms. Both persistence times and lengths are exponentially distributed at all forces, consistent with expected Poisson-type behavior, though their timescales differ at high forces. The mean run length and time increase exponentially as load force decreases below $6.5\ kT/2d$ (1.3 pN), with SKIP taking hundreds of unidirectional steps when $|F_{ext}| = |F_{99}|$ before reversing direction. We emphasize that this is achieved only by persistence of the initial direction, with no asymmetry in the track design or ligand pulse sequence. At higher load force the mean persistence time appears to plateau while the mean persistence length goes to zero. Here the run length is limited by stalling. Below $4\ kT/2d$ (0.8 pN), $P_F \approx 1$, whereby SKIP continued to move forwards for the duration of the simulations. For comparison, kinesin, considered a processive molecular motor, takes about 150 steps before detaching from its microtubule track [35, 37].

3.3. Shuttling

Because SKIP includes no asymmetry in its track design or ligand pulse sequence, persistent 'forward' and 'backward' motion are equivalent in the absence of an external force. This feature allows the interesting possibility of using SKIP as a shuttle, for example to transport cargo from one end of a track to the other end, where signals could be present to unload and pick up new cargo for reverse transportation. Such a characteristic

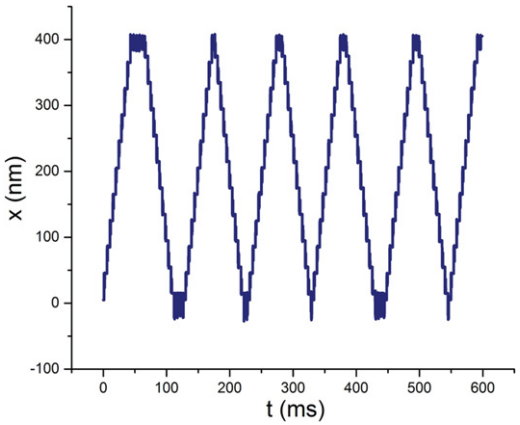

Figure 3. *Processive shuttle motion.* The track ends were each modified to possess a single *a* (*b*) site, thus restricting possible transitions from the vulnerable state (iii) to pauses and reversal, and inducing SKIP reversals at the track ends. Here, $\tau_{LP} = 0.576$ ms and $F_{ext} = 0$.

is neither possible with biological walkers such as kinesin, whose tracks possess polarity that directs motor motion, nor with previous synthetic walkers, which either exploit track polarity or alter the track as they pass. A simple modification of the track enforces the shuttling of SKIP: each end of the track has only one *a* (or *b*) binding site, so that the walker remains in the vulnerable state (figure 1(b) (iii)), diffusively searching for the reverse-binding transition (figure 1(b), R). This introduces an element of local asymmetry into the track design. A simulation of shuttling with such a track design is shown in figure 3 (see also supporting movie available at stacks.iop.org/NJP/17/055017/mmedia), illustrating that while it can take a number of pulse sequences before SKIP successfully changes direction at the end of the track, processive shuttling motion is easily achievable.

A modification of this design can establish a means by which to enforce the initial direction of SKIP. A 'localization beacon' could be included at one end of the track, with a recognition domain included in SKIP. In the absence of ligands l_a and l_b, SKIP would be driven to bind to the track at one end; upon introduction of ligand pulses SKIP would orient to move away from this end of the track. Inspired by a similar strategy used in a different synthetic motor system [30], incorporation of this beacon would enable control over the otherwise random initial orientation and location of SKIP on the track.

3.4. Performance under external feedback

As the load force increases, SKIP is increasingly less likely to continue in a forward direction. For cargo transport against a force, this is an undesirable property. From a physics point of view, this behavior does, however, provide an intriguing possibility to explore use of feedback as a means of enhancing motor performance. From information about the walker's directionality, the external force can be reversed so that it always exerts a load, thereby providing a potential means of increasing the work done against an external force by the walker. The operation of a motor in this way corresponds to an implementation of a Maxwell demon: using some mechanism to read the state of the motor (its momentary stepping direction), an external agent would take action by adjusting the direction of a load force to maximize the work extracted from the motor. It is worth noting that—strictly speaking—feedback is intrinsically needed to be able to extract work from a motor: if the initial binding configuration is random (as it would be in the absence of a localization beacon), stepping needs to be observed in order to determine the direction of motion and to choose the direction of a load force.

As a question of fundamental physics of motors, we wish to understand the energetic implications of using feedback. How well does feedback work, and what is its thermodynamic cost in terms of efficiency?

The protocols used to implement feedback are described in section 2.2 for the Langevin simulations and in section 2.3 for the Monte Carlo simulations. Once a reversal of motor direction is detected in the simulations, the direction, but not the magnitude, of the applied force is reversed so as to apply a load force opposing the new direction of motion. Figure 4(a) shows sample trajectories obtained using this feedback protocol in Langevin simulations. Up to considerable forces of several $kT/2d$, the motor executes extended runs against this force in a given direction, and rarely switches provided that the ligand pulse time is large enough. At higher forces ($|F_{ext}|$ larger than about 8 $kT/2d$, or 1.6 pN), the motor exhibits shorter runs prior to reversal, thus leading to more frequent switching of force direction. Although the motor may not move far, it performs positive work at every forward step in either direction because of this feedback. Figure 4(b) shows the accumulated work along with the time-trace of the applied force for $|F_{ext}| = 2$ pN (which corresponds to the green trace in figure 4(a)).

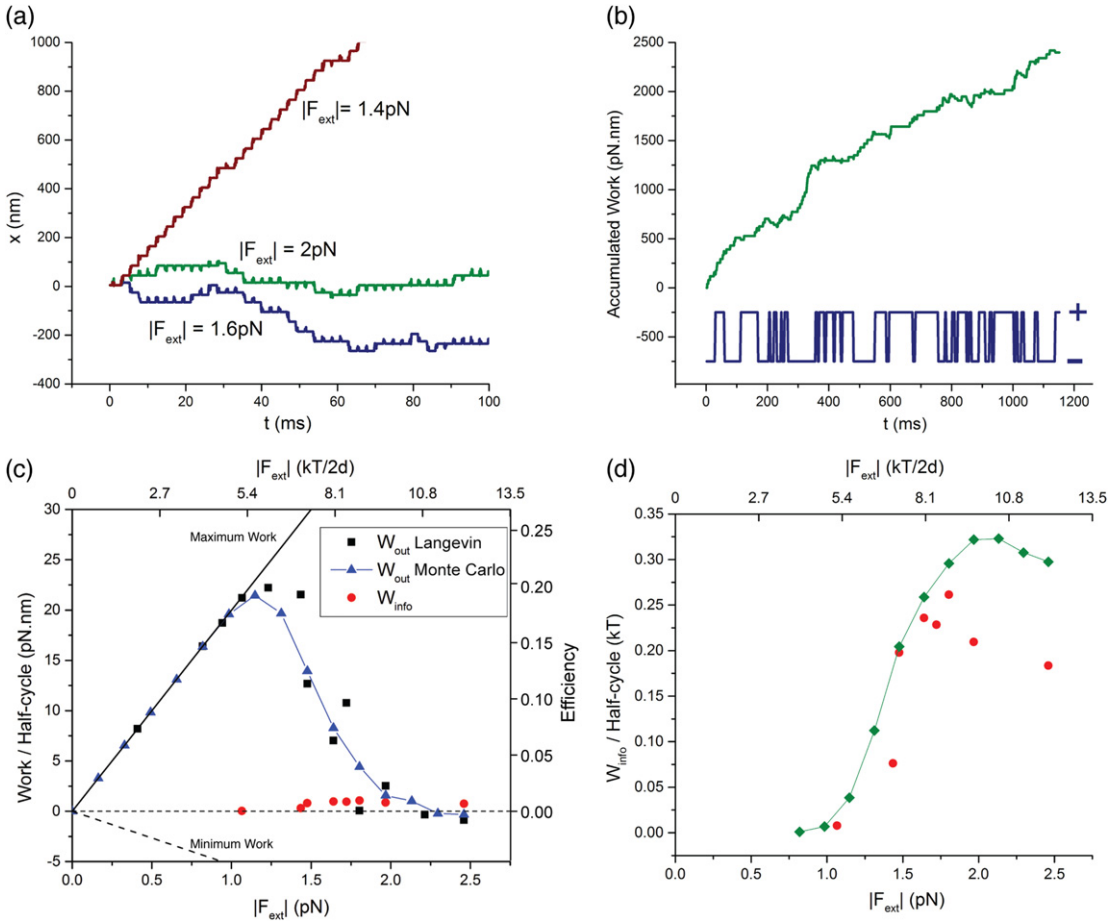

Figure 4. *SKIP feedback motor.* (a) Example trajectories of motor motion with feedback showing the initial part of each run for clarity of detail. (b) The upper green trace shows the cumulative work done by the feedback motor under a load force of 2 pN (corresponding to the green trace in panel (a)). The lower blue trace shows the direction of the load force during the simulation. Note: the timescale is an order of magnitude longer than panel (a). (c) Average output work, efficiency and information cost per half cycle ($2\tau_{LP}$) as function of load force for $\tau_{LP} = 0.576$ ms. Plotted are values of W_{out} from Langevin simulations (black squares) and from Monte Carlo simulations based on probabilities from figure 2(a) (blue triangles with connecting lines), and W_{info} derived from force switching in the Langevin feedback scheme (see text and equation (4); red circles). The thermodynamic efficiency, $\eta_{th} = W_{out}/\Delta G_{in}$, is based on the proposed implementation and does not include the information cost, which is negligible. The solid black line shows the maximum possible work (every step forwards) while the dashed line shows the minimum work (reversal at every step). (d) Expanded view of W_{info} determined from the Shannon entropy, here in units of kT, calculated two ways: from the force switching in Langevin feedback (red circles), and an upper estimate obtained using $P_R(F)$ from figure 2(a) (green diamonds).

Since negative work only occurs upon reversal transitions (rare, particularly at lower forces), this leads to a considerable amount of average work per half cycle (figure 4(c)).

The output work of SKIP operated under feedback control initially increases linearly with applied force, since reversals and pauses are rare, and so most timesteps involve F_{ext}*$2d$ of work arising from forward stepping against the force (figure 4(c)). Around F_{99}, the work per half-cycle ($2\tau_{LP}$) reaches a maximum before declining nonlinearly with applied force. This decline results from the increasingly likely transitions to pause and reversal configurations from the vulnerable state, which respectively contribute zero and negative work to the process. Nonetheless, due to the feedback algorithm, the average work per half-cycle remains positive up to reasonably high forces of magnitude greater than 2 pN.

The agreement between the shape of the work-versus-force curve from Langevin simulations and from Monte Carlo simulations provides insight into the mechanism of SKIP's motility. While the Langevin simulations inherently considered all possible transitions and changes of center-of-mass, the Monte Carlo simulations focused only on the vulnerable state, assuming that transitions from this state (figure 1(b) (iii)) were of predominant importance when explaining the force-dependent characteristics of SKIP. This assumption is validated by the reasonable agreement between the work outputs calculated using the two means of simulation (figure 4(c)). This result highlights that improvements to the performance of SKIP should focus on enhancing forward transitions from the vulnerable state under load. In kinesin, this is accomplished by a power stroke [2], whereas SKIP relies on diffusion.

Table 2. Comparison with kinesin.

	Kinesin[a]	SKIP[b]
Stall force	5.7 ± 4 pN 5.1 ± 0.5 pN	~1 pN[c]
Step size	8 nm	20 nm
Step time	~10 ms	~1 ms
Run length (steps)	125 (from [35] at 0 pN)	~600 (at F_{99} and $\tau_{LP} = 0.576$ ms)
Maximum work/step	~40 pN nm	20 pN nm
Input free energy/step	*ATP hydrolysis:* ~80 pN nm	*Chemical potential:* 113 pN nm ($m = 3$)[d] 227 pN nm ($m = 6$) 340 pN nm ($m = 9$)
Maximum efficiency	50%	18% ($m = 3$) 8.8% ($m = 6$) 5.9% ($m = 9$)

[a] Kinesin parameters based on [36] unless otherwise noted.
[b] SKIP parameters based on a half-cycle ($2\tau_{LP}$) where $\tau_{LP} = 0.576$ ms.
[c] Maximum load force is set at F_{99}.
[d] m is the order of magnitude of the ratio between high ligand and low ligand concentrations (see text).

3.5. Input energy

To estimate the energy efficiency of SKIP we need to calculate the input energy. As described briefly in section 2.1, we conceived an implementation of SKIP where stepping is achieved by periodically changing ligand concentrations using a fluidic device. The motor is then powered by moving ligand molecules from temporal regions of high chemical potential to ones with low chemical potential.

On binding to the track, two SKIP modules, *AA* (or *BB*) remove two ligands from the high ligand concentration, l_a (or l_b). During release from the track, these two modules release the ligands to a low ligand concentration. This transfer of ligands reduces the free energy difference between ligand pulse solutions. To ensure microscopic reversibility, we now assume that the ligands l_a and l_b are present in all ligand pulses, with a concentration ratio of 10^m between the 'high' and 'low' concentration conditions (i.e., if $m = 3$, then there is a 1000 fold greater concentration of l_a in (l_a, l_b) than in (0, l_b)). Assuming the ligand pulses are ideal solutions, the change in Gibbs free energy per half-cycle ($2\tau_{LP}$) is given by:

$$\Delta G_{\text{half cycle}} = -2mkT \cdot \ln 10. \tag{3}$$

Thus the free energy utilized by the motor is determined by the ratio of the high ligand concentration where the modules bind to ligands and attach to the track, to the low ligand concentration where the modules release the ligands and detach from the track.

The minimum input free energy will depend on details of motor implementation, including the τ_{LP}. Basing each track-binding module on a ligand-gated DNA-binding repressor, as per our previous design [24], would require the transfer of two ligands per module, as the repressor proteins are homodimeric. Thus the change in Gibbs free energy per half-cycle will be double the value calculated using equation (3). Our previous design of a protein-based motor that walks on a DNA track indicates that a minimum value of $m = 3$ ($\Delta G = 113$ pN nm or about 28 kT) would likely be required experimentally to enable on/off control of ligand-gated track-binding for τ_{LP} on the order of milliseconds to seconds [24].

3.6. Motor efficiency

SKIP's efficiency can be estimated from the simulation results and input energy calculations. Here we take efficiency to be the thermodynamic efficiency, $\eta_{th} = W_{out}/\Delta G_{in}$, in the absence of external feedback.

Using F_{99} as the external force, the maximum work performed by the motor in each half cycle ($2\tau_{LP} = 1.1$ ms) is on the order of 20 pN nm, or about 5 kT (table 2). The efficiency depends on the ratio between the high and low ligand concentrations as per above. If this ratio is ~10^3 ($m = 3$), then the resulting maximal efficiency will be ~18% (table 2). This is not much lower than the efficiency of the motor protein kinesin (table 2) [36], whose maximum number of steps is comparable to SKIP's directional persistence at this value of the rearward force (figure 2(d)).

Of course, if left to run for a long time under a rearward force, SKIP will eventually change direction and step assisted by the external force. Under these conditions it will do negative work, eventually erasing its gains in work (and efficiency) from stepping with an opposing force. However, positive work and hence efficiency can be regained by imposing feedback just after SKIP has reversed (see section 3.4).

When using feedback, the thermodynamic cost of recording information, W_{info}, must be taken into account, and the thermodynamic efficiency becomes $\eta_{\text{th}} = W_{\text{out}} / \left(\Delta G_{\text{in}} + W_{\text{info}}\right)$ [38]. To calculate W_{info} we transform the data for $F_{\text{ext}}(t)$ (figure 4(b)) obtained from Langevin simulations into a binary string, representing changes in the direction of the force as '1' and unchanged force as '0', and calculate the probability p of motor reversals as the number of switches divided by the number of half-cycles. The information cost can then be determined from the Shannon entropy [39] as

$$W_{\text{info}} = kT\left(-p\ln p - (1-p)\ln(1-p)\right). \tag{4}$$

This represents an upper limit to the information cost, which is exact for completely uncorrelated force switching times. If the switching probability were 50%, W_{info} would reach a maximum $kT\ln 2$ per step, which is known as the Landauer limit for information [39, 40].

Comparing W_{info} to W_{out}, we see that the information cost W_{info} is generally substantially smaller than W_{out}, except at the highest forces where pauses together with some reversals become so frequent that W_{out} goes to zero or becomes slightly negative, even in the presence of feedback (figure 4(c)). For small $|F_{\text{ext}}|$, W_{info} goes to zero because motor reversals are extremely rare, and the information content of measurements of the motor direction is essentially zero. Thus, in almost all cases, the information cost is minimal compared to the work output.

The shape of the force-dependent W_{info} curve can be interpreted in terms of the reversal probabilities. While the upper limit for W_{info} is $kT\ln 2$, our analysis reveals that, for this τ_{LP}, the maximum reached for SKIP is less than half of this value (figure 4(d)). This is consistent with the reversal probability always remaining below 0.5 (figure 2(a)). The dependence of W_{info} on force found from analysis of Langevin force switches is similar to what would be predicted from equation (4) using the force-dependent reversal probabilities P_{R} from figure 2(a). As seen in figure 4(d), however, the energy cost assuming these single-step probabilities overestimates what is found through explicit simulation. This is likely caused by the contributions of pausing to the dynamics of the system, from which entry into the reversal state is not immediately possible. This reduces the average effective reversal probability per half-cycle below P_{R} from the vulnerable state alone.

Finally, we compare the energy scales of feedback and the free energy we estimate to run the motor. From this, we find that the motor efficiency is negligibly affected by the thermodynamic cost of feedback. This is because W_{info} is bounded from above by $kT\ln 2 \approx 2.8$ pN nm per step, which is much smaller than the ΔG_{in} of at least 113 pN nm required for the repressor-based implementation of SKIP. It can therefore be inferred from figure 4(d) that the thermodynamic efficiency is very little altered by the incorporation of W_{info}, and therefore has the same force dependence as the output work (figure 4(c), right-hand axis). Implementing feedback in this experimental conception of SKIP is seen to have no significant cost and substantial benefits.

4. Discussion and interpretation

SKIP is an unusual molecular walker in that its track is spatially symmetric and the ligand pulse sequence controlling its dynamics is symmetric in time. As such, in the absence of additional orientational cues, the initial direction of SKIP is arbitrary. Once set in motion, the motor is directional and processive under moderate load conditions (load forces of several $kT/2d$).

The maximum load force against which SKIP can work increases with τ_{LP} (figure 2(b)). Naturally, this increase in cycle time results in a decrease in power output. For practical implementation, one must decide between optimizing for efficiency or for power. Furthermore, practical limitations, such as the natural lifetimes of track-bound modules A and B, will restrict the range of timescales for τ_{LP}, such that the output work cannot become arbitrarily large.

The concept of SKIP as introduced in this work is quite general: one needs to have feet of addressable stickiness, which could in principle be achieved through means other than the ligand-exchange proposed here, such as photoswitching [27] or self-sustaining oscillating chemical reactions [41, 42]. While certain results presented herein are specific to the repressor-based design (such as the free energy input driving the system to move), other findings are more general. For example, the energetic cost of feedback could contribute more substantially to the efficiency of experimental realizations of SKIP that are driven by a lower free energy input than the chemical potential of ligand exchange in this protein design.

In the long-time limit on a long track, SKIP should not be classified as a molecular motor, but rather as a persistent random walker, i.e., a walker whose directionality persists over many cycles, but can switch randomly and increasingly as force opposes its motion. Thus, the long-time limit of its behavior is expected to become diffusive. While control over its initial direction would enable the extraction of useful work over shorter track lengths at low to moderate forces, feedback could be implemented for longer tracks and/or higher forces due to the non-zero probability of reversal of motion, thus transforming the walker to a motor after reversal. It is

important to note that the predicted length of SKIP's persistent walk is so long at low enough rearward force ($|F_{ext}| < |F_{99}|$) and large enough values of the ligand pulse time that for all intents and purposes, its directional persistence away from a specified end on an experimentally realistic track length will provide, on average, motor-like properties. This is because the probability of reversal for $|F_{ext}| < |F_{99}|$ is close to zero [43].

The performance of SKIP as determined from our simulations compares favorably with the processive protein motor kinesin that inspired its design. Table 2 shows experimental values for kinesin based on single-molecule measurements [35, 36]. For the parameters used in our simulations, SKIP exhibits exceptional processivity and persistence of its direction, particularly at low force where it can take >1000 steps in a given direction before reversing. This is an order of magnitude more steps than typical run lengths of kinesin [35]. It is important to note that our simulations disregard practical aspects of an experimental implementation of SKIP, such as non-specific binding and realistic binding constants for ligands to repressors and repressors to their DNA-binding motifs [44].

Because of the symmetry inherent in its design, SKIP can behave as a shuttle, where the design of the ends of the track can cause the walker to reverse direction automatically. In this sense, SKIP has a capability lacking in its biological inspiration: bidirectional transport of cargo along microtubules requires the presence of both kinesin and the oppositely-directed dynein motors, while SKIP can transport cargo bidirectionally and processively between two ends of a reasonably-sized track.

Our concept of SKIP is focused on its operation as an individual walker on a single track. The ability of multiple SKIPs interacting to transport a common cargo will most likely be much poorer than the cooperative transport by multiple polar walkers such as kinesin [45]. This question remains for future investigations. Here we focus on comparing the single-molecule properties of SKIP with those of kinesin.

Our simulations use a SKIP τ_{LP} that is an order of magnitude shorter than the shortest average kinesin step time of 10 ms; nonetheless a comparison of other motor properties is insightful. For example, SKIP will continue to move in a forward direction at rearward forces (F_{99}) that are about 20% of the kinesin stall force. However, the SKIP step size is 20 nm (cf 8 nm for kinesin). Thus the net maximum work is similar (40 and 20 pN nm for kinesin and SKIP, respectively). We have set this larger step to allow construction of SKIP using known ligand-dependent DNA binding proteins [24].

The Gibbs free energy utilized by SKIP per step is similar to the free energy of the kinesin ATPase reaction. Thus the efficiency of SKIP as calculated by the simulations is of the same order as that of kinesin (50% versus 18% for kinesin and SKIP, respectively).

The comparison between kinesin and SKIP shows that it should be possible to construct a protein motor that transduces energy via a ratchet mechanism only and has a performance and efficiency that is similar to real protein motors. The comparison with kinesin suggests that a portion of its mechanochemical energy transduction may be via a ratchet mechanism. Thus, it may be possible to extract significant energy in the form of directed work out of protein-based walkers that lack allosteric coupling and whose motion between ratchet sites arises only from random thermal diffusion.

Acknowledgments

We acknowledge financial support from the Human Frontier Science Program (RGP0031/2007). MJZ wishes to thank the IRMACS Centre at Simon Fraser University for availability of workspace and IRMACS, the Westgrid Computer Network and Compute Canada for use of computing facilities. He also thanks David Lee of the SFU Physics Department for making several videos of SKIP's motion, one of which is shown in the supplementary information available at stacks.iop.org/NJP/17/055017/mmedia. NRF acknowledges the Pacific Institute for the Mathematical Sciences (PIMS) for hosting a sabbatical visit, and financial support from an NSERC Discovery Grant. HL acknowledges support from the Swedish Research Council, nmC@LU, and a Visiting Research Fellow Award from the University of New South Wales. RS and HL acknowledge support from the EU FP7 FET project INFERNOS (project no. 308850). We thank John Bechhoefer, James Walsh, Juan Parrondo and David Sivak for fruitful discussions.

References

[1] Kull F J and Endow S A 2013 *J. Cell Sci.* **126** 9–19
[2] Vale R D and Milligan R A 2000 *Science* **288** 88–95
[3] Friel C T and Howard J 2012 *J. Muscle Res. Cell Motil.* **33** 377–83
[4] Sweeney H L and Houdusse A 2010 *Annu. Rev. Biophys.* **39** 539–57
[5] Ha T, Kozlov A G and Lohman T M 2012 *Annu. Rev. Biophys.* **41** 295–319
[6] Allemand J F, Maier B and Smith D E 2012 *Curr. Opin. Biotechnol.* **23** 503–9
[7] Enemark E J and Joshua-Tor L 2008 *Curr. Opin. Struct. Biol.* **18** 243–57
[8] Ait-Haddou R and Herzog W 2003 *Cell Biochem. Biophys.* **38** 191–214

[9] Reimann P 2002 *Phys. Rep.* **361** 57–265
[10] Astumian R D 1997 *Science* **276** 917–22
[11] Howard J 1995 *Biophys. J.* **68** 245S–53S (www.ncbi.nlm.nih.gov/pmc/articles/PMC1281936/pdf/biophysj00062-0252.pdf)
[12] Vale R D and Oosawa F 1990 *Adv. Biophys.* **26** 97–134
[13] Astumian R D 2012 *Nat. Nanotechnology* **7** 684–8
[14] Astumian R D 2010 *Biophys. J.* **98** 2401–9
[15] Xie P 2011 *Theor. Biol. Med. Modelling* **8** 22
[16] Gu M and Rice C M 2010 *Proc. Natl Acad. Sci. USA* **107** 521–8
[17] Guo Q and Sousa R 2006 *J. Mol. Biol.* **358** 241–54
[18] Belyy V and Yildiz A 2014 *FEBS Lett.* **588** 3520–5
[19] Howard J 2006 *Curr. Biol.* **16** R517–9
[20] Bier M 2007 *Bio. Syst.* **88** 301–7
[21] von Delius M and Leigh D A 2011 *Chem. Soc. Rev.* **40** 3656–76
[22] Bath J and Turberfield A J 2007 *Nat. Nanotechnology* **2** 275–84
[23] Kelly T R 2005 *Angew. Chem.* **44** 4124–7
[24] Bromley E H C *et al* 2009 *HFSP J.* **3** 204–2012
[25] Loh I Y, Cheng J, Tee S R, Efremov A and Wang Z S 2014 *Acs Nano* **8** 10293–304
[26] Wang Z 2007 *Proc. Natl Acad. Sci. USA* **104** 17921–6
[27] Cheng J, Sreelatha S, Hou R, Efremov A, Liu R, van der Maarel J R and Wang Z 2012 *Phys. Rev. Lett.* **109** 238104
[28] Samii L, Blab G A, Bromley E H C, Linke H, Curmi P M G, Zuckermann M J and Forde N R 2011 *Phys. Rev.* E **84** 031111
[29] Samii L, Linke H, Zuckermann M J and Forde N R 2010 *Phys. Rev.* E **81** 021106
[30] Lund K *et al* 2010 *Nature* **465** 206–10
[31] Pei R, Taylor S K, Stefanovic D, Rudchenko S, Mitchell T E and Stojanovic M N 2006 *J. Am. Chem. Soc.* **128** 12693–9
[32] Kovacic S, Samii L, Woolfson D N, Curmi P M G, Linke H, Forde N R and Blab G A 2012 *J. Nanomaterials* **2012** 109238
[33] Niman C S, Beech J P, Tegenfeldt J O, Curmi P M G, Woolfson D N, Forde N R and Linke H 2013 *Lab Chip* **13** 2389–96
[34] Kuwada N J, Zuckermann M J, EHC B, Sessions R B, PMG C, Forde N R, Woolfson D N and Linke H 2011 *Phys. Rev.* E **84** 031922
[35] Block S M, Asbury C L, Shaevitz J W and Lang M J 2003 *Proc. Natl Acad. Sci. USA* **100** 2351–6
[36] Svoboda K and Block S M 1994 *Cell* **77** 773–84
[37] Thorn K S, Ubersax J A and Vale R D 2000 *J. Cell Biol.* **151** 1093–100
[38] Cao F J and Feito M 2009 *Phys. Rev.* E **79** 041118
[39] Cao F J and Feito M 2012 *Entropy* **14** 834–47
[40] Jun Y, Gavrilov M and Bechhoefer J 2014 *Phys. Rev. Lett.* **113** 190601
[41] Novak B and Tyson J J 2008 *Nat. Rev. Mol. Cell Biol.* **9** 981–91
[42] Noyes R M and Field R J 1974 *Annu. Rev. Phys. Chem.* **25** 95–119
[43] Efremov A and Wang Z 2011 *Phys. Chem. Chem. Phys.* **13** 5159–70
[44] Kuwada N J, Blab G A and Linke H 2010 *Chem. Phys.* **375** 479–85
[45] Uppulury K, Efremov A K, Driver J W, Jamison D K, Mr D and Kolomeisky A B 2013 *Cell. Mol. Bioeng.* **6** 38–47